Contents

1 Integer Quantum Hall Effect (IQHE) 1
1.1 Classical Hall Effect 1
1.2 Quantum Hall Effect (QHE) 2
1.2.1 Realization of 2D electron gas 2
1.3 Theory of QHE 3
1.3.1 Explanation for the quantization 6
1.4 Resistance standard 9

2 The Finnish resistance standard based on QHE at VTT 9
2.1 Cryogenic Current Comparator (CCC) 10
2.2 Error sources 14
2.3 Ratio error of the CCC 15
2.4 Ratio error of primary and secondary currents 15
2.5 Compensation current sources 15
2.6 QHE component 16
2.7 Other systematic errors 16
2.8 Random uncertainty 16
2.9 Conclusion of the error 16

3 Experimental values 17

4 Concluding remarks 17

1 Integer Quantum Hall Effect (IQHE)

1.1 Classical Hall Effect

The Hall effect has been known for a long time. The name is after E.H. Hall (1855–1938), who was a professor at Harvard University from 1881 to 1921. The Hall effect can be seen in a situation as in figure 1, where the magnetic flux density $\mathbf{B}$ ($||\mathbf{z}$) is perpendicular to the probe and current flows along the probe ($||\mathbf{x}$) perpendicular to $\mathbf{B}$. Hall-voltage is measured in the y-direction between the opposite sample edges. This phenomenon, where voltage is induced in perpendicular direction to the magnetic field and current, is known as the Hall phenomenon.

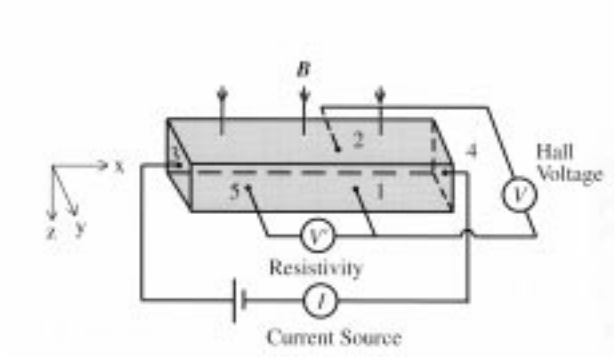

Fig. 1 The Hall geometry.

The Hall phenonmenon can be understood when we start with the classical Lorentz-force equation

$$m^* \frac{d^2 r}{dt^2} + \frac{m^*}{\tau} \frac{dr}{dt} = (-e)[\mathbf{E} + (\mathbf{v} \times \mathbf{B})], \tag{1}$$

where m^* is the effective mass and τ denotes the relaxation time of an electron in a magnetic field with the flux density $\mathbf{B}$ and the electric field $\mathbf{E}$. When we take the steady state solution $\frac{d^2 r}{dt^2} = 0$ and the magnetic field to be parallel to the z-axis, i.e, $\mathbf{B} = (0, 0, B_z)$ and use the definition of the current density $\mathbf{j} = n(-e)\mathbf{v}$ we will get equations:

$$j_x = \sigma_0 E_x - \omega_c \tau j_y, \tag{2}$$

$$j_y = \sigma_0 E_y + \omega_c \tau j_x, \tag{3}$$

$$j_z = \sigma_0 E_z, \tag{4}$$

where $\omega_c \equiv eB_z/m^*$ is the classical cyclotron frequency of the electron in the presence of the magnetic field B_z, and $\sigma_0 = ne^2\tau/m^*$ is the zero field conductivity. In steady state it is obvious that the current $j_y = 0$, which gives us from Eq. (3)

$$E_y = -\frac{\omega_c \tau j_x}{\sigma_0} \tag{5}$$

and from Eq. (2)

$$j_x = \sigma_0 E_x. \tag{6}$$

By defining the Hall-resistance as $\rho_{xy} \equiv \frac{|E_y|}{j_x}$, we will have for our geometry the result

$$\rho_{xy} = \frac{\omega_c \tau}{\sigma_0} = \frac{B_z}{ne}. \tag{7}$$

We see that ρ_{xy} depends linearly on B_z. Hall measurements can be used i.e. to measure the density of electrons n [1].

1.2 Quantum Hall Effect (QHE)

The QHE was discovered in 1980 by Klaus von Klitzing et. al. [2]. The qeometry in the experiment is the same as in the Hall-effect, but **the magnetic field is strong, temperature low** ($\hbar\omega >> k_B T$) **and the electron gas is two-dimensional**. Under these conditions the Hall-resistance curve developed plateaus as in figure 2, and the phenomenon was given the name Quantum Hall Effect.

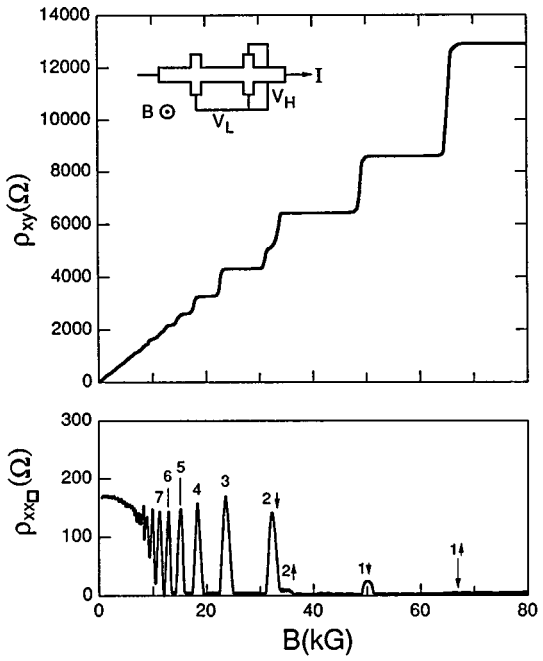

Fig. 2 The QHE measurement curve.

1.2.1 Realization of 2D electron gas

In the first experiment the two dimensional electron gas was realized in a metal-oxide-semiconductor-field-effect-transistor (MOSFET). Figure 3 presents the picture of the MOSFET and its energy diagram. When the gate voltage of the MOSFET is positive with respect to the semiconductor, a very thin inversion layer forms under the SiO_2 and it attracts electrons and they form a two dimensional electron gas.

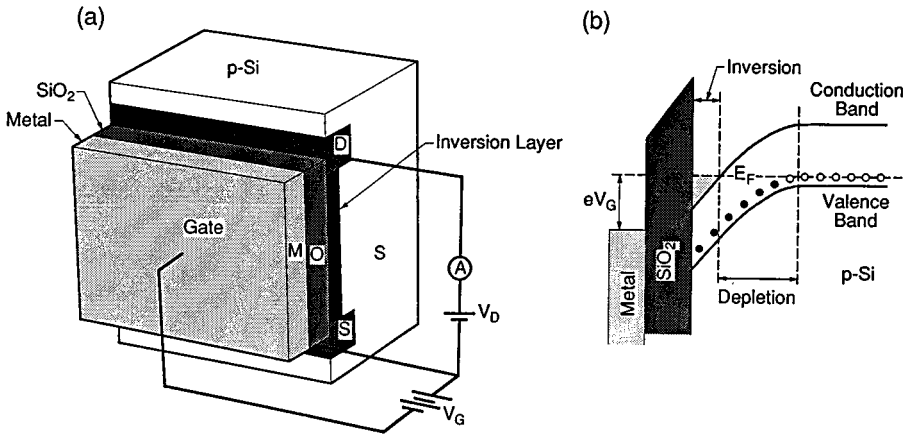

Fig. 3 a) QHE sample made out of a MOSFET. b) Energy band diagram of the MOSFET, where we can see the inversion layer which traps the 2D electron gas.

The QHE has also been realized in $Al_xGa_{1-x}As/GaAs$ samples. The energy diagram of an AlGaAs/GaAs sample is shown in figure 4 [3, 4, 5].

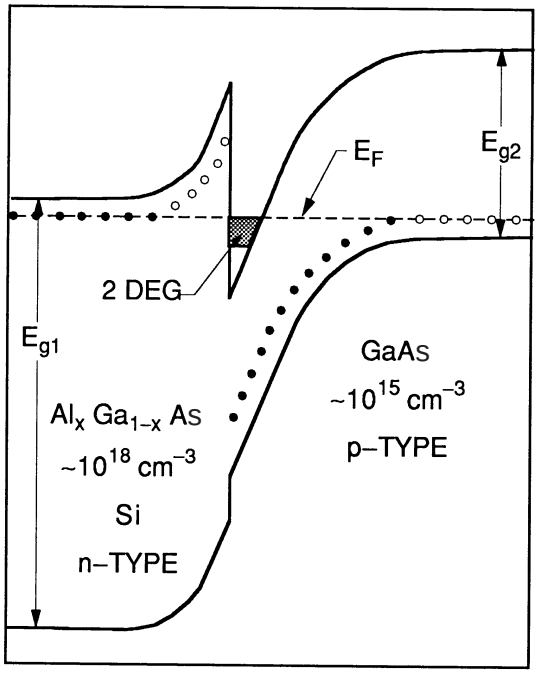

Fig. 4 The energy band diagram of a $Al_xGa_{1-x}As/GaAs$ -sample

1.3 Theory of QHE

We start with the Schrödinger equation for an electron in a magnetic field $\mathbf{B} = \nabla \times \mathbf{A}$

$$\{\frac{1}{2m^*}[-i\hbar\nabla + e\mathbf{A}]^2 + U\}\Phi = E\Phi. \tag{8}$$

At the beginning we take the potential energy $U = 0$ and use the Landau gauge for the vector potential $\mathbf{A} = (0, Bx, 0)$ which gives us

$$\frac{1}{2m^*}[p_x^2 + (p_y + eBx)^2]\Phi = E\Phi. \tag{9}$$

The eigenfunction can be separated to have a plane-wave solution $\exp(ik_y y)$ which yields

$$\frac{1}{2m^*}[p_x^2 + (p_y + eBx)^2]e^{-ik_y y}\Psi = Ee^{-ik_y y}\Psi. \tag{10}$$

We may then replace p_y with $\hbar k_y$ and we will have

$$\frac{1}{2m^*}[p_x^2 + (\hbar k_y + eBx)^2]\Psi = E\Psi. \tag{11}$$

This can be written as

$$-\frac{\hbar^2}{2m^*}\Psi'' + \frac{1}{2}m\omega_c^2(x - X)^2\Psi = E\Psi \tag{12}$$

$$X \equiv -k_y l_0^2,\ l_0^2 \equiv \frac{\hbar}{eB},\ \omega_c = \frac{eB}{m^*}.$$

l_0 is called the magnetic length. Equation (12) has exactly the same form as the quantum-mechanical harmonic oscillator where X is the equilibrium position of the harmonic potential. Thus we get the harmonic oscillator solution with the plane-wave factor in y-direction:

$$\Phi_{k_y,n} = e^{-ik_y y}\exp[\frac{-(x - X)^2}{2l_0^2}]H_n[(x - X)/l_0], \tag{13}$$

where $H_n[x]$ is the nth order Hermitian polynom. We see that the wave-functions are highly localized in x-direction, but extend as plane-waves in y-direction. They are like 'spaghettis' parallel to the y-axis. For energy eigen-values we get the standard solution

$$E_n = (n + \frac{1}{2})\hbar\omega_c. \tag{14}$$

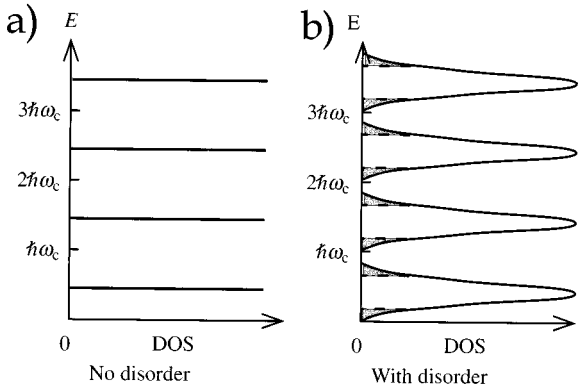

Fig. 5 a) The DOS of a 2D electron gas is made of δ-functions separated by a distance $\hbar\omega_c$.b) In real samples the δ-functions broaden because of the impurity potential $U \neq 0$.

For a 2D electron gas the Density Of States (DOS) with respect to the energy is $\frac{dn}{dE} = \frac{m^*}{\pi\hbar^2}$ and is constant, unlike in the 3D case ($\propto \sqrt{E}$) or in the 1D case ($\propto 1/\sqrt{E}$). We see that, by turning the magnetic field on, our DOS will change from constant to the constant times δ-functions which have the name Landau levels. The new DOS is illustrated in figure 5.

To calculate the degeneracy of the Landau levels we start with the standard box-normalization for the plane waves in y-direction, which gives us

$$k_y = \frac{2\pi}{L_y} m, \tag{15}$$

where m is an integer and L_y is the y-dimension of the sample. This gives

$$\Delta k_y = \frac{2\pi}{L_y} \tag{16}$$

for the separation between k_y values. Next we calculate how many states there are in the whole sample in subband n by calculating the number of localized states in the x-direction, i.e.

$$N = L_x/\Delta x, \tag{17}$$

where L_x is the x-dimension of the sample. N is calculated with the help of Δk_y while X depends on that variable. We will have

$$\Delta x = |X(k_y + \Delta k_y) - X(k_y)| = l_0^2(k_y + \Delta k_y - k_y) = l_0^2 \Delta k_y = \frac{h}{eBL_y}. \tag{18}$$

Using Eq. (17) we will get N, the number of the states on a Landau level:

$$N = \frac{L_x L_y}{h} eB, \tag{19}$$

and n_L, the density of electrons of a filled Landau level:

$$n_L = \frac{N}{L_x L_y} = \frac{eB}{h}. \tag{20}$$

We use the electron density of the whole sample n_s and define the filling factor ν as the number of the sub-bands filled

$$\nu = \frac{n_s}{n_L} = \frac{n_s h}{eB}. \tag{21}$$

Now we turn on the electric field E_x which is due to the potential difference between the edges of the sample. The electric field can be described with potential

$$U(x) = eE_x x. \tag{22}$$

By using the identity

$$\frac{1}{2}m^*\omega_c^2(x-X)^2 + eE_x x = \frac{1}{2}m^*\omega_c^2(x-[X-\frac{eE_x}{m^*\omega_c^2}])^2 - \frac{1}{2}m^*\omega_c^2[\frac{eE_x}{m^*\omega_c^2}]^2 + \frac{m^*\omega_c^2}{2}2X\frac{eE_x}{m^*\omega_c^2} \tag{23}$$

we see that the centers of the wavefunctions shift sideways

$$X(k_y) \rightarrow X(k_y) - \frac{eE_x}{m^*\omega_c^2} = X'(k_y), \tag{24}$$

which gives a new solution

$$\Phi(X) \rightarrow \Phi(X'). \tag{25}$$

The energy eigenvalues change to

$$E \rightarrow E' = (n + \frac{1}{2})\hbar\omega_c + eE_x X' + \frac{m^*}{2}(\frac{E_x}{B})^2. \tag{26}$$

Now we may proceed further to get the current density j_y by calculating the drift velocity of the electrons in the y-direction

$$v_y = < \Phi(X')|\frac{1}{m^*}(-i\hbar\frac{d}{dy} - eA_y)|\Phi(X') > = \frac{1}{m^*}(\hbar k_y - eBX'(k_y)) = \frac{E_x}{B}. \tag{27}$$

From this relation we can calculate the current density j_y

$$j_y = env_y = en\frac{E_x}{B} = \frac{e\nu}{2\pi l_0^2}\frac{E_x}{B} = \nu\frac{e^2 E_x}{h}, \tag{28}$$

and this gives finally expression for the Hall resistivity

$$\rho_{xy} = \frac{E_x}{j_y} = \frac{h}{\nu e^2}. \tag{29}$$

This doesn't explain yet why the resistivity has the plateaus while the filling factor ν is a continuous function of the magnetic field and the electron density.

1.3.1 Explanation for the quantization

In the derivation above we didn't take boundary conditions into account. Actually the Landau-levels approach infinity in the proximity of the sample edges. This is illustrated in figure 6, where it is obvious that when E_f lies between Landau levels, there are only 1D edge channels transporting the current. We may think a situation, where the chemical potetials μ of the two electron reservoirs (the drain and the source) differ by a value $\delta\mu$. This potential difference is the driving force for the current flow and is the voltage difference times e between the reservoirs.

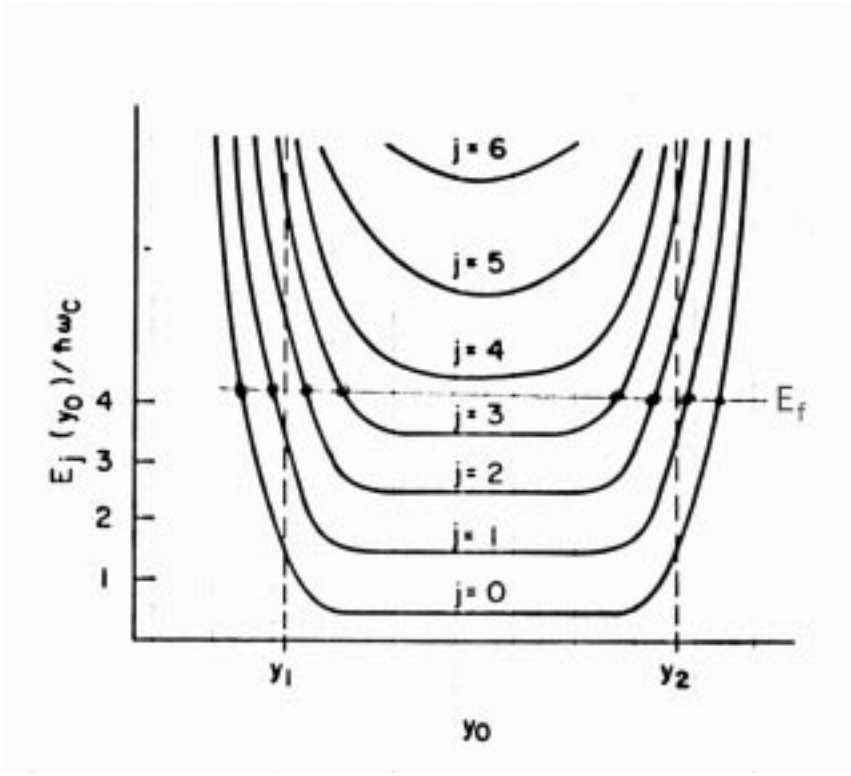

Fig. 6 The energy levels of an rectangular object in perpendicular magnetic field.

In 1D case the DOS in k-space is

$$\frac{dn}{dk} = (2\pi)^{-1}. \tag{30}$$

The current of one 1D channel i is

$$j_i = 2e \int_{E_f}^{E_f+\delta\mu} \frac{dn}{dE} v(E) dE. \tag{31}$$

The factor 2 comes from the spin degeneracy. By using the semiclassical model of electron dynamics [7]

$$v(E) = \frac{1}{\hbar}\frac{dE}{dk}, \tag{32}$$

and the identity using Eq. (30)

$$\frac{dn}{dE} = \frac{dn}{dk}\frac{dk}{dE} = \frac{1}{2\pi}(\frac{dE}{dk})^{-1}, \tag{33}$$

we can rewrite (31) as

$$j_i = 2e \int_{E_f}^{E_f+\delta\mu} \frac{1}{2\pi}(\frac{dE}{dk})^{-1}\frac{dE}{\hbar dk} dE = \frac{2e}{h}\int_{E_f}^{E_f+\delta\mu} dE = \frac{2e}{h}\delta\mu. \tag{34}$$

Thus we have the conductance G of M number of 1D channels:

$$G = \frac{I}{V} = \frac{eI}{\delta\mu} = M\frac{2e^2}{h}, \tag{35}$$

where we have used the identities $\delta\mu = eV$ and $I = \sum_{i=0}^{M} j_i = M2e^2/h\delta\mu$. This equation is equal to a 2-terminal Landauer formula: $G = \frac{2e^2}{h}\sum_{n=1}^{M} T_n$, where transmission propabilities T_n=1 [8, 9, 10].

Our situation is now such that we have 1D channels in the edges of the sample. There is nearly no overlap of the wavefunctions of the different sides of the sample and therefore we may ignore the scattering between the states. We have a situation like in the figure 7 where the current flows from the right reservoir to the left or from the left to the right. It is matter of bookkeeping which side carries the current, depending whether we consider holes or electrons.

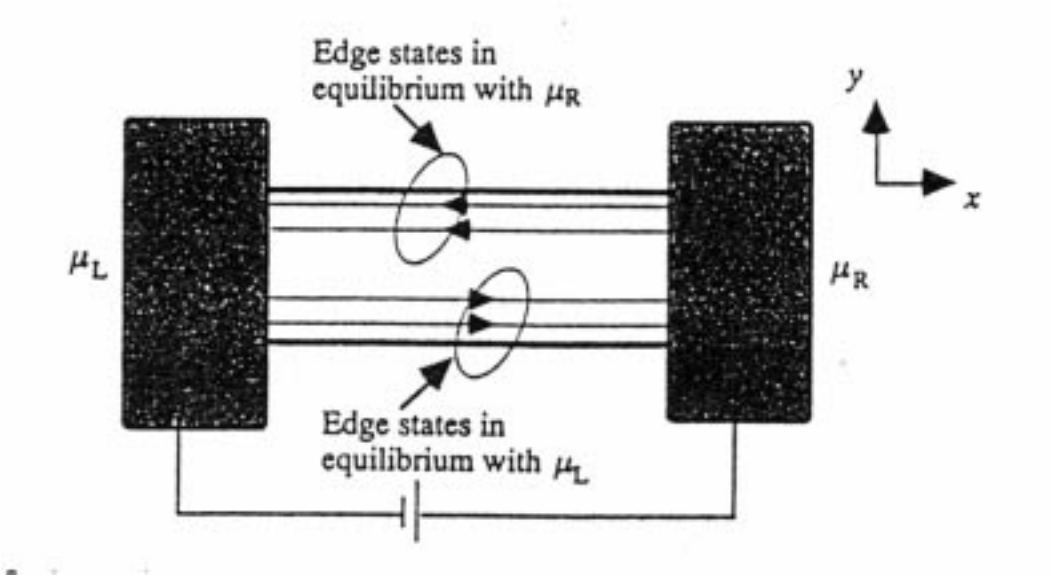

Fig. 7 The edge currents and their chemical potentials which depends on from which reservoir the current originates.

While there is no scattering, the chemical potential μ is constant in the channel and thus there is not any longitudinal voltage difference. First when a charge carrier enters the target reservoir there is scattering which adjusts carrier's energy to the chemical potential of that reservoir. Thus there is a voltage difference between the channels at opposite edges, while the channels originate from different reservoirs at different chemical potentials. If we now calculate the Hall resistance we get using Eq. (35)

$$\rho_{xy} = \frac{V_y}{I_x} = \frac{h}{2e^2 M}. \tag{36}$$

At high magnetic fields the spin up and down states apart due to their Zeeman energy and the factor 2 is removed from the denominator in the previous formula [11]. Thus we have plateaus in ρ_{xy} at values which corresponds to integer fractions of

$$\frac{h}{e^2} = 25812.8056\Omega \equiv R_{K-90}, \tag{37}$$

within an accuracy of at least 10^{-8}. This constant was called as one Klitzing in 1990 when the resistance standard was defined.

1.4 Resistance standard

The best measurements of R_{K-90} are accurate to 0.045 ppm with respect to other SI-units. This means that a least-squares fit has been made with many independent measurements against the other units and the uncertainty corresponds to the standard devitation of the fits. The measurement of R_{K-90} itself reproduces values with an accuracy of 0.01 ppm, and thus the higher uncertainty is due to the fit process with base units [12]. When we reproduce resistance from the SI units without QHE we will have the uncertainty of $2 \cdot 10^{-7}$. There we use the definition of the one ohm resistance

$$1\Omega = 1m^2 \cdot 1kg \cdot s^{-3} \cdot A^{-2}. \tag{38}$$

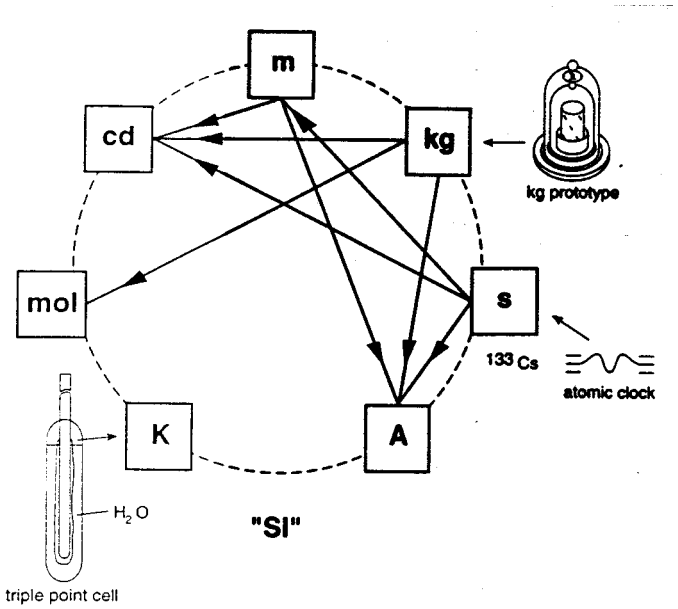

Fig. 8 The base units of the SI.

Figure 8 illustrates the relations of some basic SI units. From Eq. (38) it is obvious that resistance is defined with respect to one kilogram standard mass and ^{133}Cs atomic clock second. Since QHE gives smaller uncertainty, the resistance is defined nowadays with the QHE method [6].

2 The Finnish resistance standard based on QHE at VTT

In this section I will describe how a QHE resistance standard is implemented at VTT[1] [13] .

[1]VTT Automation, Measurement technology, FIN-02044 VTT, Finland.

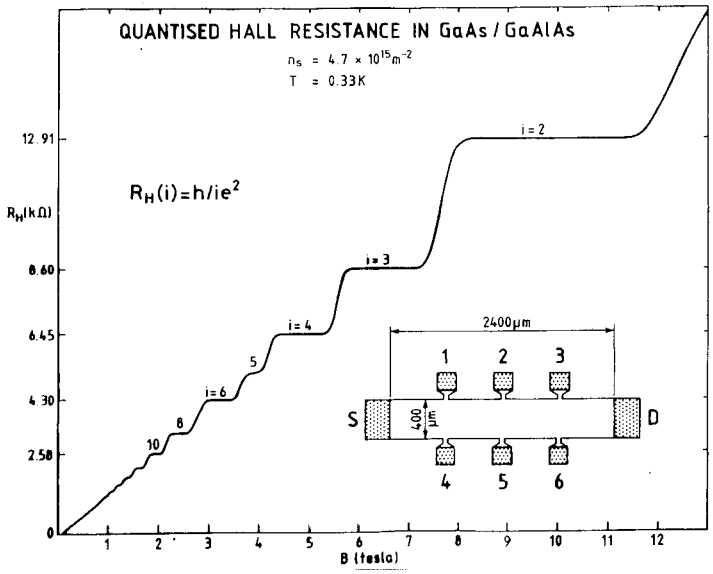

Fig. 9 The QHE-based resistance standard of VTT. The inset shows the sample geometry, where current flows from the source (S) to the drain (D) and the Hall voltage is measured between one of the pairs 1-4, 2-5, 3-6.

The QHE measurement of VTT is shown in figure 9. The resistance standard is measured in the middle of the flat region near the filling factor ν=2.

It is not enough to have an accurate QHE-resistor. Once the accurate resistor can be compared accurately to another resistor, we have an accurate system to measure resistance. For this purpose VTT uses a Cryogenic Current Comparator (CCC) to measure the ratio of two currents: the first going through the unknown resistor R_x and the second going trough the QHE sample. When the voltage difference over the resistors is the same as measured with a Superconducting QUantum Interference Device (SQUID), the current ratio determines the resistance ratio:

$$\frac{I_{QHE}}{I_x} = \frac{R_x}{R_{QHE}}. \tag{39}$$

2.1 Cryogenic Current Comparator (CCC)

With a cryogenic current comparator the ratio of two currents can be determined with extremely high accuracy. The high accuracy is due to the perfect diamagnetic properties of the superconducting shields while the high sensitivity is achieved by sensing the net current linkage with SQUIDs [14, 15].

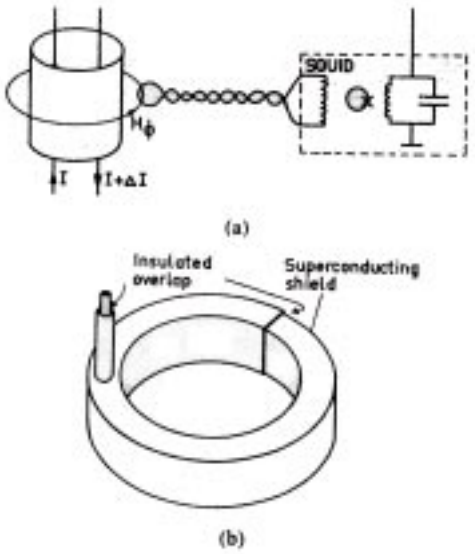

Fig. 10 (a) The basic idea of the CCC. (b) A practical realization of the CCC called the overlapped-tube comparator.

The basic idea of the CCC can be understood by looking at figure 10a. Two currents flow into opposite directions through an infinitely (in this first model) long superconducting shield. Because the magnetic field inside the thick superconducting shield must be zero, the inner tube must carry resultant current ΔI on its inner surface. The current must return (over the end of the tube) on the outer surface in the direction of the original net current. That means we have the current difference on the surface what can be measured by coupling the magnetic flux induced by the surface current to a SQUID. When the measured flux is null, the currents are equal.

In figure 10b is a finite implementation of the CCC called the overlapped-tube comparator. There the current flows inside a torus in opposite directions, which induces the net current on the superconducting torus surface. The magnetic flux is measured inside the torus and when it's zero the currents are equal. It's to be noted that there is an insulated overlap where the tube goes inside itself like a snake eating its tail, which introduces a small error to the measurements. The overlap is to allow the current flow from inside to the outside surface.

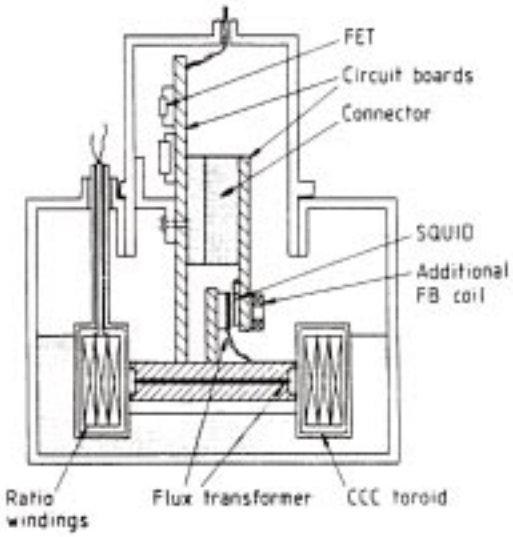

Fig. 11 The CCC geometry used in the QHE resistance measurements.

The geometry that is used in the QHE resistance measurements is shown in figure 11. The CCC contains different ratios of windings: 8, 16, 16, 32, 64, 393, 609, 768 and 886 which enables to create ratios: 1:1, 1:1.2906, 1:10, 1:100 and 1:129.0625. The current resolution achieved is 68 pA turn/$\sqrt{Hz}$

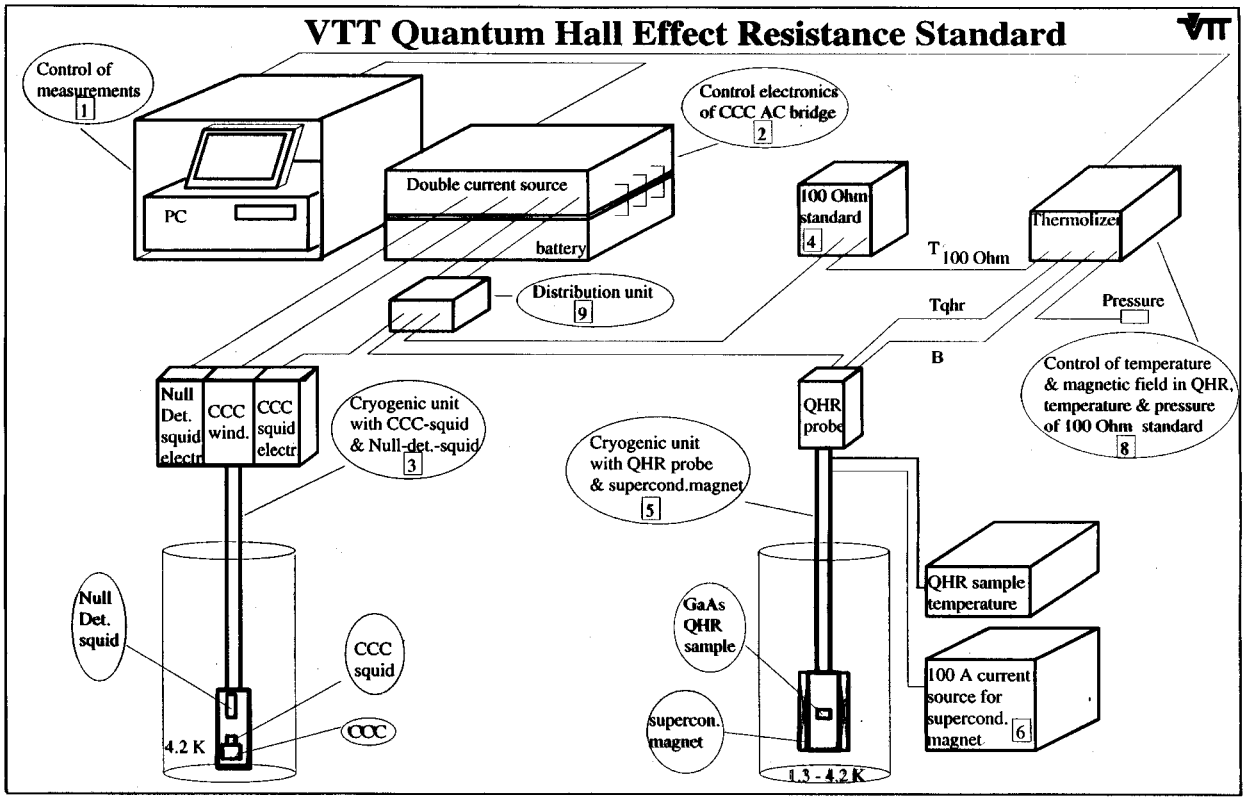

Fig. 12 The measurement configuration.

Figure 12 illustrates the different components of the whole measurement configuration. The measurement is controlled with a PC-computer. One of the currents of a double current source flows through the QHE-sample and the

other through the compared 100 Ω resistance standard. The temperature and pressure of the standard resistance are kept constant. The two currents are compared with the CCC and, with feedback, a zero net current in the CCC is searched.

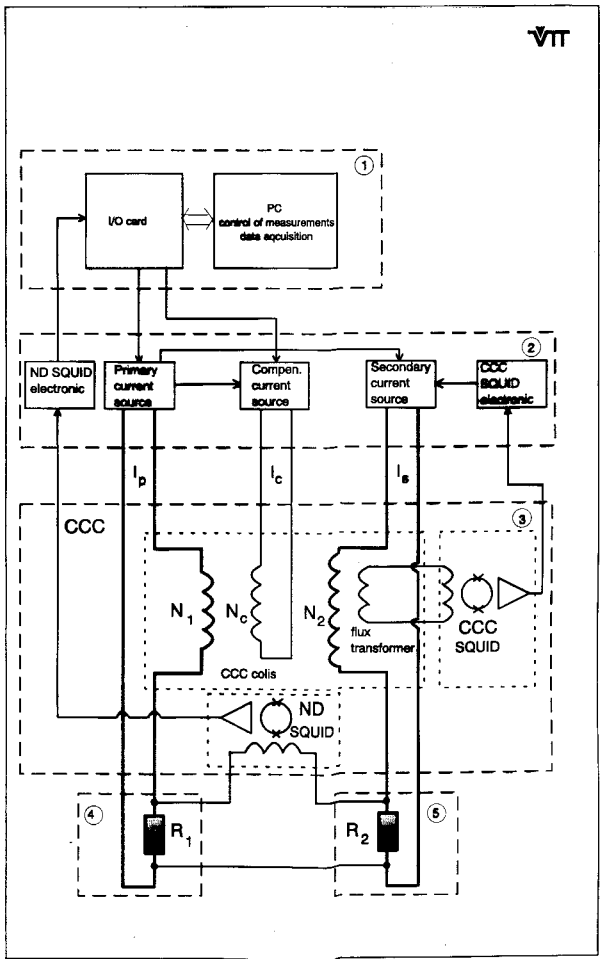

Fig. 13 The block diagram of the measurement configuration.

A more detailed description of the system is shown in figure 13. We start to analyze the figure from the middle where the null detector (ND) SQUID is located. This is used to measure the potential difference between the resistors. The feedback is made so that a zero difference between the potential over the resistors is achieved. R_1 is the QHE-based resistor and R_2 the unknown one. The output of the ND SQUID goes through a proportional-integrator (PI) controller to the computer, which controls the primary current source (PCS) to null the potential difference between the resistors. While the winding ratio N_2:N_1 is naturally little different from the resistance ratio

$$\frac{R_1}{R_2} = \frac{I_S}{I_P}, \tag{40}$$

a compensating current I_C is introduced to cancel the flux from the N_1I_p-N_2I_S. The flux is zero when

$$N_1 I_p - N_2 I_S = N_C I_C. \tag{41}$$

Thus we get using Eqs. (40) and (41)

$$\frac{R_1}{R_2} = \frac{N_1 + N_C I_C / I_P}{N_2}, \tag{42}$$

and we see that by using a low ratio for N_C:N_2 and I_C:I_P we can measure accurately the ratio R_1:R_2. A CCC SQUID is used to get the null position of the CCC flux by using a $PI^{3/2}$ controller to control the secondary current source (SCS). A more detailed schematic diagram of the system is presented in figure 14.

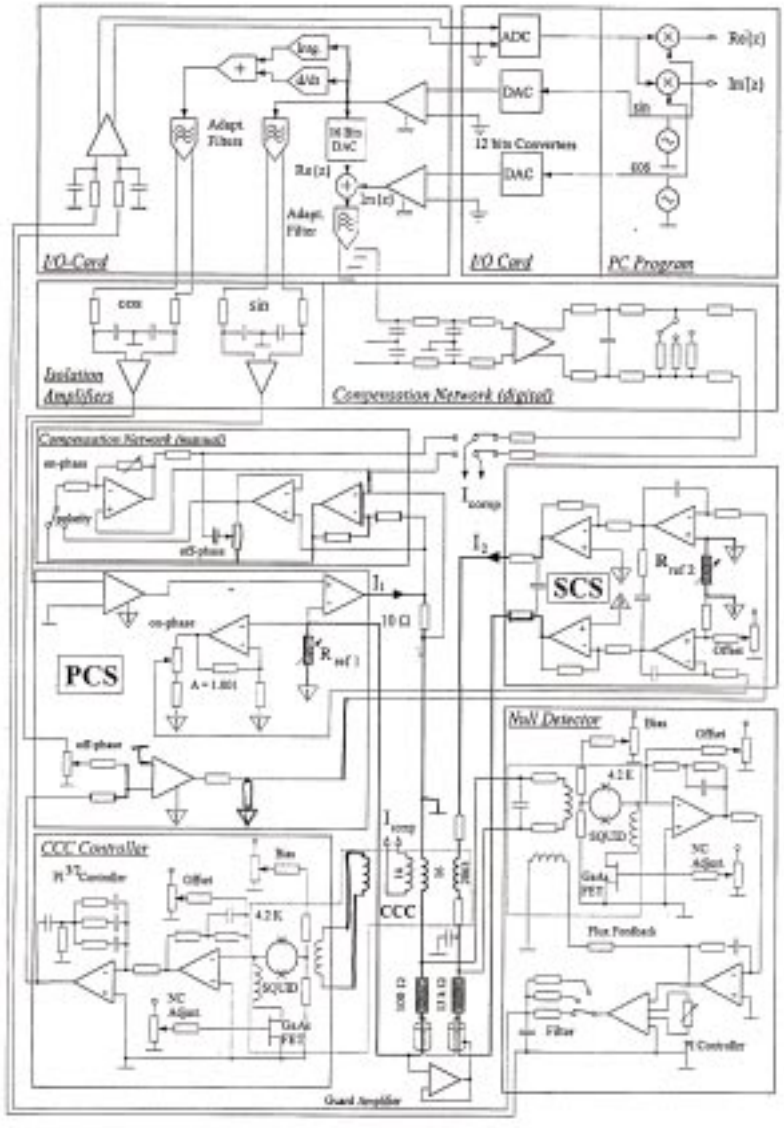

Fig. 14 The schematic diagram of the measurement configuration.

2.2 Error sources

When the QHE-based resistance measurement is made with the CCC-based resistance bridge several sources of errors appear [16]. The biggest ones are the systematic errors since random uncertainties can be eliminated by time integration.

2.3 Ratio error of the CCC

In the ratio windings there is a stray capacitance C_{stray}. The current through the stray capacitance depends on the frequency and it is given by:

$$I_C = I_2(\frac{f}{f_{LC}})^2,\ f_{LC} = \frac{1}{(2\pi)^2 LC_{stray}}. \tag{43}$$

In this configuration $f_{LC} \approx 35$ kHz and the measurement frequency is about 1Hz, giving an error

$$e_{stray} = (f/f_{LC})^2 < 1ppb. \tag{44}$$

The non-ideality of the CCC geometry gives rise to an error. If b is the thickness of the cap between overlaps, R_t the radius of the toroidal CCC, l the lenght of the overlap, l_y the width of the rectangular type CCC, we have expression for the error which we denote as the dc-ratio-error

$$e_{dc} = \frac{b}{\pi R_t} e^{-\pi l/l_y} / \ln(\pi R_t/l_y). \tag{45}$$

In the VTT geometry the error is

$$e_{dc} < 0.5ppb. \tag{46}$$

Thus, total ratio error e_{CCC} is

$$e_{CCC} < 1.5ppb. \tag{47}$$

2.4 Ratio error of primary and secondary currents

By using a phase-sensitive detector the current ratio can be measured within 1 ppm. Actually a value of 5 ppm is more realistic due to the misadjustment and the drift of the current ratio. By using a controller with an open loop gain $A(f)$, the error can be reduced by the factor $1/A(f)$. For a PI-controller $|A(f)| \approx (f_{cut}/f)$, where f is the measurement frequency and f_{cut} is the cutoff frequency of the controller. With an optical isolation amplifier f_{cut} is limited to be under 1kHz. This gives a 5 ppb at 1Hz measurement frequency. With a $PI^{3/2}$-controller which has an open-loop gain $|A(f)| \approx (f_{cut}/f)^{3/2}$, the error can be further reduced by a factor of 30. In most cases the error is neglible

$$e_{prim:sec} < 0.3ppb. \tag{48}$$

2.5 Compensation current sources

The estimated size of the digitally controlled source is 100 ppm with an uncertainty of 50 ppm. This gives a maximum error of

$$e_{comp} < 5ppb. \tag{49}$$

2.6 QHE component

The error e_{HALL} can be defined as

$$e_{HALL} = s\frac{\rho_{xx}}{\rho_{xy}}. \tag{50}$$

In most cases $\rho_{xx} <$ 0.4 mΩ, and when $\rho_{xy} \approx$ 13 kΩ

$$e_{HALL} \lesssim 3 - 30ppb. \tag{51}$$

The constant s, which measures how well the Hall voltage probes are perpendicular to the current, is usually much smaller than 1. At low temperatures no temperature dependence is observed. The current dependence of e_{HALL} is measured to be 0.05 – 1 ppb/μA when the current was varied in the range of 10 – 50 μA. The error is then

$$e_{HALL} < 0.01ppm, \tag{52}$$

when current is less than 30 μA.

2.7 Other systematic errors

The error due to the leakage current between sources is

$$e_{leakage} < 1ppb. \tag{53}$$

Twisted coaxial cables, whose outer shields are actively guarded, are used to eliminate the error due to the dc leakage resistance, which can be given a relation

$$e_{dc-leakage} < 0.5ppb. \tag{54}$$

2.8 Random uncertainty

The resolution of the CCC, the null detector, the thermal noise of the resistors gives some random uncertainty, but this is with the 10 min integration time of the order

$$e_{ru} < 0.001ppm \tag{55}$$

and can thus be neglected.

2.9 Conclusion of the error

The biggest error $\approx$ 0.01ppm is systematic in its origin and caused by the QHE sample itself. Thus the measurement configuration can't be any better without a different kind of a sample or different physics.

3 Experimental values

The measured values of the VTT QHE resistance at different times are shown in figure 15. The resistance was compared in 1994 to the French standard by transporting the secondary resistance standard with an air-plane. We see that in long run the resistance has an accuracy of 0.05 ppm and over a shorter period of time 0.01ppm [17].

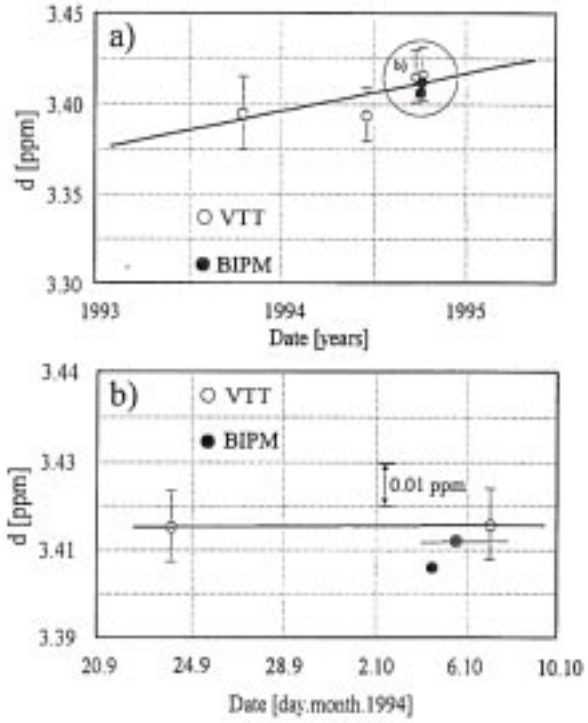

Fig. 15 The VTT measured QHE resistance compared to the French standard as a function of time

4 Concluding remarks

QHE phenomenon is used succesfully to implement the resistance standard with an accuracy of 0.01 ppm and the VTT implementation gets the measured accuracy to that level.

I have to thank Alexandre Saprapinski and Aarne Oja for discussion about the measurement system and for the material.

References

[1] P. Y. Yu and M. Cardona, *Fundamentals of Semiconductors: Physics and Materials Properties*, (Springer, Berlin, 1996).

[2] K. von Klitzing, G. Dorda, M. Pepper, Phys. Rev. Lett. **45**, 494 (1980).

[3] *T. M. Rice, Festkörperphysik II (Solid-State physics II) Lecture notes*, ETH Zürich (1996), (unpublished).

[4] T. Chakraborty and P. Pietiläinen, *The Quantum Hall effects*, *Springer series in solid-state sciences 85*, 2 ed. (Springer, Berlin, 1995).

[5] J. Arponen, *Statistinen Fysiikka (Statistical Physics)*, (Limes, Helsinki, 1994).

[6] D. King and T. Quinn, "Metrology: Quo Vadis ?",*IEEE Trans. Instr. Mes* **44**, 86 (1995).

[7] N.W. Ashcroft, and N.D.Mermin, *Solid State Physics*, (Saunders, Philadelphia, 1976).

[8] R. Landauer, IBM J. Res. Dev. **1**, 223 (1957).

[9] R. Landauer, Phys. Lett. **85A**, 91 (1981).

[10] R. Landauer, J. Phys. Condens. Matter **1**, 8099 (1989).

[11] S. Datta, *Electronic Transport in Mesoscopic Systems*, (Cambridge, New York, 1995).

[12] E. R. Cohen, and B. N. Taylor, "The Fundamental Physical Constants", *Physics Today*, BG 9 August (1996).

[13] H. Seppä and A. Satrapinski, "AC Resistance Bridge Based on the Cryogenic Current Comparator", *IEEE Trans. Instr. Mes.* **2**, 463 (1997).

[14] H. Seppä, "The Ratio Error of the Overlapped-Tube Cryogenic Current Comparator" , *IEEE Trans. Instr. Mes.* **39**, 689 (1990).

[15] H. Seppä and A. Satrapinski, "A Cryogenic Current Comparator Based On a Low-noise DC SQUID and a DC Coupled Readout Electronics", CPEM'92, 9–12 June, Paris-France, (1992).

[16] H. Seppä, A. Satrapinski, T. Varpula, and J.–M. Saari, "Frequency Dependence of 100-Ω Standard Resistors Measured with a CCC-Based AC Resistance Bridge", *IEEE Trans. Instr. Mes.* **44**, 276 (1995).

[17] H. Seppä and A. Satrapinski, "Determination of Ω_{VTT} using the Quantum Hall Resistance", CPEM'96, 17–20 June, Braunschweig Germany (1996).